Surface & Coatings Technology 420 (2021) 127326

Contents lists available at ScienceDirect

Surface & Coatings Technology

journal homepage: www.elsevier.com/locate/surfcoat

Microstructure and indentation hardness study of CAE-PVD (Cr,Ti,Al)N solid solution coatings deposited using a combinatorial multitarget approach

Gonzalo G. Fuentes *, Lucía Pérez-Gandarilla, Angel Medrano, José Fernández Palacio, Rebeca Bueno, Eduardo Arias-Egido, Jonathan Fernández

Center of Advanced Surface Engineering, AIN, Cordovilla-Pamplona E31191, Spain

ARTICLE INFO

Keywords:
CrTiAlN coatings
Wear
Cathodic arc evaporation

ABSTRACT

In this study we have analysed the indentation hardness and modulus of cathodic arc deposited CrTiAlN coatings as a function of the stoichiometric variables Ti/Cr, Al content and cation mix. The coatings have been prepared using a combinatorial cathode composition approach, leading up to 14 different stoichiometries produced in 5 batches. The coatings have been inspected by glow discharge optical emission spectroscopy, scanning electron microscopy, X-ray diffraction and nanoindentation techniques. The coatings develop crystalline structures compatible with solid solutions of face–centered cubic unit cells for all the compositions produced. Such unit cells exhibited a downwards lattice parameter dependency on the aluminum concentration of the coatings (from 0.417 nm down to 0.413 nm). The indentation hardness as a function of the Ti/Cr is compatible with other previous studies reported. The films hardnesses and moduli also increase as the aluminum concentration increases (21 GPa up to 34 GPa). Both indentation responses upon Ti/Cr and Al are attributed to solid solution strengthening. However in order to prove this statement, the indentation hardness and modulus were studied as a function of the mixing term of the cations, as this term is well representative of the solid solution compositional map. The observed results unambiguously evidence that the solid solution strengthening effect is confirmed on the basis of the dependency between the indentation hardness and the so called degree of mixing.

1. Introduction

Physical vapour deposition (PVD) of quaternary coating systems such as CrTiAlN have received the attention of the researchers due to their good performance in high speed machining and other tooling applications [1–5]. Earliest reference of this coating formulation begins in the first decade of the 2000s [4,5], using sputtering and arc plating techniques as deposition methods. Essentially, the vacuum reactive deposition of Ti, Cr and Al metals in nitrogen gas leads to nearly perfect fcc-crystalline solid solutions for a wide range of coating stoichiometries. Only for Al concentration as high as 70at% other secondary phases such as h-AlN may nucleate and grow. That observation obeys to the fact that both Ti and Cr form nitrides of the same unit cell structure (i.e. face–centered cubic), and that these cells allow a high solubility of Al, which is located at cation substitutional sites.

The high solubility of Al and the presence of Cr provides the CrTiAlN coating system with high hardness, excellent oxidation resistance and structural stability even at high temperatures [6–10].

Such outstanding performance and its correlation with the coating microstructures have been studied and characterized extensively; for example, Zhou et al. [7] and Yamamoto et al. [8] found that the microstructure of high Al content CrTiAlN remained unaltered after annealing at 900 °C in air. Above this temperature, mixtures of cubic and hexagonal phases were formed. Hasegawa et al. [11] observed that the CrTiAlN cubic-type films partially transformed to hexagonal structure by annealing over 900 °C. More recently, Chen et al. [12] investigated the thermal decomposition of CrTiAlN alloy coatings at 1000 °C–1100 °C, identifying different decomposition routes through nucleation and growth of h-AlN, c-TiN and c-CrAlN phases.

The indentation hardnesses and modulus of CrTiAlN coating formulations obtained by different PVD methods have also been reported in the literature [1–15], observing, in overall, similar dependencies on the ratio between the cationic constituents. Specifically, most of the reported studies indicate that the hardness and modulus of CrTiAlN

* Corresponding author at: Center of Advanced Surface Engineering, AIN, Carretera de Pamplona, 1, Cordovilla E31191, Spain.
E-mail address: gfuentes@ain.es (G.G. Fuentes).

https://doi.org/10.1016/j.surfcoat.2021.127326
Received 22 February 2021; Received in revised form 3 May 2021; Accepted 18 May 2021
Available online 24 May 2021

coatings increase as the ratio of Ti over Cr [9,10] or over Cr + Al [13] increases, regardless of the deposition method used. For example, we (Georgiadis et al. [13]) found a correlation between the lattice parameter $\mathbf{a_0}$ and the indentation hardness of CAE deposited films, both increasing as the Ti/(Cr + Al) cation ratio increased, although the correlation was inferred only with a limited number of tested specimens. Similar correlations between hardness and Ti concentration were also found by Y. Xu et al. [9]. Zhou et al. [7] and Danek et al. [10] also reported that the hardness of the CrTiAlN sputtered coatings decreased as the Cr content increased, which aligns with Refs [9,13]. On the other hand, Lin et al. [6] reported a sharp increase in hardness up to 40 GPa for Ti atomic fractions of 11%, in hybrid high power impulse magnetron sputtering (HiPIMS) CrTiAlN coatings, attributed to different factors such as solid solution strengthening and (111) preferred plane lattice orientation.

The fracture toughnesses of sputtered CrTiAlN on Si substrates have also been characterized [14], whilst the friction properties of CrTiAlN coatings investigated by different authors [4–7,13,15,16,17]. In general terms, it is found that coefficients of friction (COFs) ranges between 0.5 and 0.7, using counter balls of bearing steel, WC or Al_2O_3, showing in some reported cases a slight decrease of the coefficients of friction at room temperature as the Cr-atom concentration increases over Ti [17].

Generally speaking, most of the studies carried out on the indentation hardness of the system CrTiAlN are based on a limited number of specimens analysed; between 3 and 6 to 7. That fact could be valid to highlight partial dependencies of hardness and modulus as a function of compositional parameters (typically Ti/Cr atom ratio), though it may omit other compositional dependencies. In this study we have produced and qualified a larger number of specimens (up to 14), using a combinatorial approach that have allowed to get a variety of cation atomic compositions. Such approach has already been implemented by other authors for similar or other coating systems (see for example [12,18]) to further unveil correlations between microstructures and mechanical responses. We have explored the indentation hardness and modulus against (i) the more classical atom ratio Ti/Cr to compare the results with these previously published, (ii) the absolute Aluminum concentration; and additionally (iii) as a function of the degree of 'mixed-upness' or simply mixing [19] that a crystalline structure may exhibit when *Z*-different atomic constituents randomly locate in the available lattice sites of a solid solution. All that with the purpose to discuss the possible mechanisms of film strengthening as a function of the stoichiometry for this quaternary coating system. We have not found, to the best of our knowledge, any recent study in which such correlation had been attempted experimentally on any quaternary nitride coatings or on any with higher number of constituents (some of these called high entropy nitride coatings [20,21]).

2. Experimental

2.1. Coating deposition

A set of 14-combinatory compositional (Cr,Ti,Al)N coatings have been produced by cathodic arc evaporation in a commercial PVD reactor. A scheme of the evaporation set up is inserted at the right-hand side column of Table 1. The reactor is equipped with 2 opposing columns, each of them hosting 3 circular cathodes (10 cm diameter) aligned vertically. Both columns face each other and leave an effective volume of 0.5 m^3 available for the substrates located at the centre of the chamber. For the preparation of the coatings, the left-side column was equipped with pure Ti cathodes. This column has the purpose to carry out ion bombardment pretreatment on the test samples and to produce an adhesion TiN film before the CrTiAlN film deposition. The right-side column was prepared with various combinations of cathode compositions in order to investigate the properties of the deposited coatings as a function of the proportions of the Me constituents Cr, Ti and Al. The cathode positions of the right side are labelled as *top*, *middle* and *bottom* (cf. Table 2). 5 different batches were prepared, each hosting 3 or 4 subsets of test specimens located at different heights of the sample holder namely again *top*, *middle*, *bottom* and very *bottom*. The top positioned samples coincide approximately in height with the top positioned cathodes. Table 1 indicates the composition of the different cathodes used for every batch/position. The targets utilized were single or bimetal of 99.8 wt% purity of 70 mm diameter.

The substrates were hot work H13 steels (53–55 HRc) with a chemical composition of 0.4at%C, 0.9at%Si, 0.3at%Mn, 5.43at%Cr,

Table 2
Deposition parameters for the coating batches.

Phase 1: Ar^+ bombardment (AEGD)	
Substrate bias (V)	−600
Pressure Ar (Pa)	1
Anode voltaje (V)	60
Phase 2: Ti^+ bombardment (AEGD)	
× 3 Ti current (A)	60
Substrate bias (V)	−600
Phase 3: TiN adhesión layer	
Substrate bias (V)	−60
Ti based arc current (A)	45
Pressure PN_2 (Pa)	1
Phase 4: deposition CrTiAlN films	
Cr based arc current (A)	60
Ti based arc current (A)	45
Substrate bias (V)	−60
Pressure PN_2 (Pa)	4
Temperature °C	420–440

Table 1
Cathode composition and relative location in the reactor chamber for each of the 5-coating batches.

Batch	Cathode position	Cathode composition/(amperage)	Sample set code	Scheme of cathode and sample positioning in the reactor chamber
1	Top	Ti (45)	A (top)	
	Middle	$Cr_{0.3}Al_{0.7}$ (60)	B (middle)	
	Bottom	–	C (bottom)	
2	Top	Ti (45)	A (top)	
	Middle	$Cr_{0.5}Al_{0.5}$ (60)	B (middle)	
	Bottom	–	C (bottom)	
3	Top	Ti (45)	A (top)	
	Middle	Cr (60)	B (middle)	
	Bottom	$Cr_{0.3}Al_{0.7}$ (60)	C (bottom)	
4	Top	Cr (60)	A (top)	
	Middle	$Ti_{0.33}Al_{0.67}$ (45)	B (middle)	
	Bottom	–	C (bottom)	
	–	–	D (very bottom)	
5	Top	$Cr_{0.3}Al_{0.7}$ (60)	A (middle)	
	Mid bottom	$Ti_{0.33}Al_{0.67}$ (45)	–	
	Bottom	–	–	

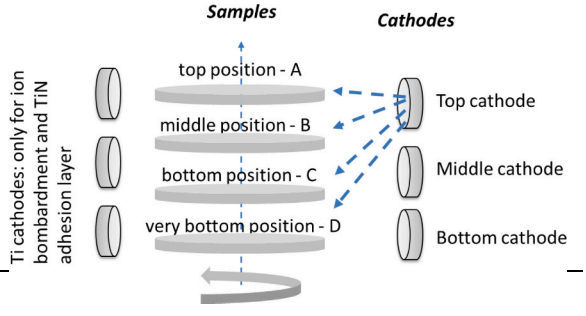

1.32at%Mo, and 0.96at%V. Discs of 30 mm diameter were mirror polished (Ra < 15 nm) and cleaned in ultrasonic bath using de-oiling agents and de-ionised water. Si wafers were also used to inspect the specimen cross sections in the electron microscope.

The processes were initiated at a base pressure of 2×10^{-4} Pa. The subsequent steps are indicated in the form of phases on Table 2, where all relevant process parameters are displayed. The substrates were vacuum-heated and Ar^+-ion bombarded using the so called Arc Enhanced Glow Discharge (AEGD) process [22]; it is indicated as phase 1 on Table 2. In phase 2 the samples were further bombarded with Ti^+ ions at energies of 600 eV for 10 min, with the purpose to enhance the adhesion strength of the films. In phase 3, TiN adhesion layers of around 0.2 μm thick were deposited in a similar way for all the coatings. Finally phase 4 ran the specific quaternary coating depositions. For this latter phases 3 and 4, high purity N_2 gas were fed in the reactor chamber using a mass flow of 200 sccm, leading to a work pressure of 4 Pa. A continuous DC bias of −50 V was applied on the substrates during the deposition phases 3 and 4. During all the process, the substrates were rotated around the central vertical axis of the reactor chamber at a speed of 3 rpm. The substrate temperature was set to 450 °C, as measured using the tempering curve of 100Cr6 bearing steel discs, on which Vickers hardness were measured after each coating process [23].

2.2. Coating characterization

Coating composition were measured by glow discharge optical emission spectroscopy (GDOES) using a JY 10000 system equipped with radio frequency (RF) etching mode. The coating adhesions were tested using a Rockwell C indentation device and protocol followed by the visual inspection of the imprint (so call Mercedes test). The adhesion qualification is set from HF1 (very good adhesion without adhesive nor cohesive film failures) up to HF5 (total delamination around the imprint).

X-ray diffraction (XRD) was carried out in a BRUKER-D8 spectrometer in the parallel beam configuration using a Cu X-ray source (lambda = 0.154 nm) and a grazing angle of the incident beam of 0.2°. The measurement of the coating biaxial stresses was attempted using the $\sin^2\psi$ method. Although the obtained results did not allow a precise quantification, it was inferred that the coatings developed compressive stresses. A field emission scanning electron microscope (SEM) HITACHI S-4800, equipped with a secondary electron detector was used to inspect the cross sections of the films.

The indentation Hardness (H) and reduced Young modulus ($E' = E/(1-\nu^2)$) of the coatings were determined by nanoindentation using a NanoIndenter XP (MTS) with a *Berkovich* diamond tip. The tip was calibrated on a fused silica sample using the Oliver and Pharr method [24]. The measurements of H and E' as a function of the indentation depth were carried out using the Continuous Stiffness Measurement (CSM) operation mode. The drift rate was measured to be below 0.080 $nm{\cdot}s^{-1}$. The indentations were carried out at a constant strain rate of 0.05 N/s up to a maximum load of 10 N. The measurements were averaged over 20 indents for each sample. Surface Roughness was measured with a WYCO-RST 500 profilometer using the vertical scanning interferometry (VSI) mode, providing a vertical resolution of 3 nm.

3. Results & discussion

3.1. Composition and microstructure

Table 3 gathers the chemical composition of all the coatings as measured by GDOES. For each specimen the values of the Ti/Cr atomic ratio, the indentation hardness and the indentation modulus are also displayed. In addition, Table 3 also shows the calculation of the so called mixing term $-\Sigma\chi_i \times \ln\chi_i$, in which χ_i represents the atomic fraction of each of the metals (cations) of the coatings, which shall be discussed later. In the present calculation, the summation is made over the three metals Ti, Cr and Al. In all the cases, the stoichiometries recorded are compatible with Me-N compositions of unit cells with fcc cubic symmetry, where the sum of the cation compositions (Me) to the anion (N) ratio approaches the unity. Some of the specimens exhibited nitrogen concentrations below 50at%, indicating the formation of anion vacancies during growth.

Figs. 1a-e show the cross section images of various representative coatings of the series, as acquired by SEM in secondary emission electron mode. At the top-right corner of each picture, Figs. 1 show the imprint left by a Rockwell-C indenter on the coated steel specimens (these latter correspond to optical images), following the procedures of the Mercedes tests for coating adhesion. All images reveal circular cracks around the imprint zone, caused by the fracture of the coating during the large strain of the H13 steel substrate. According to the test, all the coatings are qualified as HF1 and HF2, corresponding to well adhered films.

The cross section images reveal microstructures conformed by small size dense compact columns. The microstructures of the coatings cross sections **1A** to **3A** exhibit a strong texture, in contrast to these of their TiN adhesion layers, which are less structured. In the case of the specimens **4A** and **5A**, it is observed a more evident microstructure continuity between the adhesion layer and the quaternary coating. In the case of the specimens **1A** to **3A**, the strong texture can be attributed to the small grain size reached during the growth process, which is a side effect of a poor atomic diffusion. For the specimens **4A** and **5A**, the larger grain column sizes could indicate larger atomic diffusivity during growth.

Fig. 2 shows the diffraction patterns of the deposited coatings. All patterns reveal that the coating lattice structures are formed by face centred cubic unit cells, as expected for TiN [25], CrN [26] in general, and AlTiN [27,28], AlCrN [29,30] for Al-concentrations smaller than 70at.% typically. All samples reveal the planes (111,002) and (022), in

Table 3
Stoichiometry, thickness, and hardness and indentation modulus of the 5 batches of coatings batches **1–5**. The atom ratio Ti/Cr, and the mixing term $-\sum_i^N \chi_i \times ln\chi_i$ are indicated.

Sample	Stoichiometry	Thickness (μm)	Ti/Cr ratio	$-\Sigma\chi_i\ln\chi_i$	H (GPa)	E' (GPa)
1A	$Cr_{0.13}Ti_{0.15}Al_{0.20}N_{0.52}$	2.7 ± 0.2	1.15	7.23	29.9 ± 1.0	247.4 ± 13
1B	$Cr_{0.20}Ti_{0.04}Al_{0.27}N_{0.50}$	2.7 ± 0.1	0.2	6.67	33.7 ± 3.0	247.4 ± 13
1C	$Cr_{0.22}Ti_{0.02}Al_{0.28}N_{0.48}$	1.4 ± 0.1	0.09	6.37	32.0 ± 2.2	219.2 ± 7
2A	$Cr_{0.25}Ti_{0.10}Al_{0.18}N_{0.46}$	3.5 ± 0.1	0.39	7.32	30.6 ± 1.0	197.9 ± 5
2B	$Cr_{0.30}Ti_{0.02}Al_{0.22}N_{0.46}$	4.0 ± 0.1	0.07	6.38	30.3 ± 1.4	194.8 ± 4
2C	$Cr_{0.31}Ti_{0.01}Al_{0.21}N_{0.47}$	2.0 ± 0.1	0.04	6.11	28.8 ± 3.2	238.8 ± 12
3A	$Cr_{0.39}Ti_{0.09}Al_{0.02}N_{0.50}$	2.3 ± 0.1	0.23	5.49	21.4 ± 1.4	121.3 ± 4
3B	$Cr_{0.43}Ti_{0.02}Al_{0.05}N_{0.50}$	3.0 ± 0.1	0.03	4.80	25.8 ± 1.4	193.2 ± 7
3C	$Cr_{0.37}Ti_{0.01}Al_{0.14}N_{0.48}$	2.4 ± 0.1	0.01	5.43	26.5 ± 1.0	153.4 ± 3
4A	$Cr_{0.51}Ti_{0.04}Al_{0.08}N_{0.36}$	2.9 ± 0.1	0.07	5.62	29.9 ± 2.8	243.0 ± 17
4B	$Cr_{0.29}Ti_{0.08}Al_{0.15}N_{0.48}$	2.9 ± 0.1	0.27	6.99	30.1 ± 4.3	256.5 ± 28
4C	$Cr_{0.23}Ti_{0.13}Al_{0.22}N_{0.42}$	2.8 ± 0.1	0.56	7.74	30.2 ± 4.4	271.4 ± 7
4D	$Cr_{0.11}Ti_{0.19}Al_{0.31}N_{0.39}$	1.7 ± 0.1	1.73	7.66	34.5 ± 3.9	275.5 ± 26
5A	$Cr_{0.12}Ti_{0.07}Al_{0.39}N_{0.42}$	2.7 ± 0.1	0.55	6.73	27.8 ± 3.1	260.1 ± 25

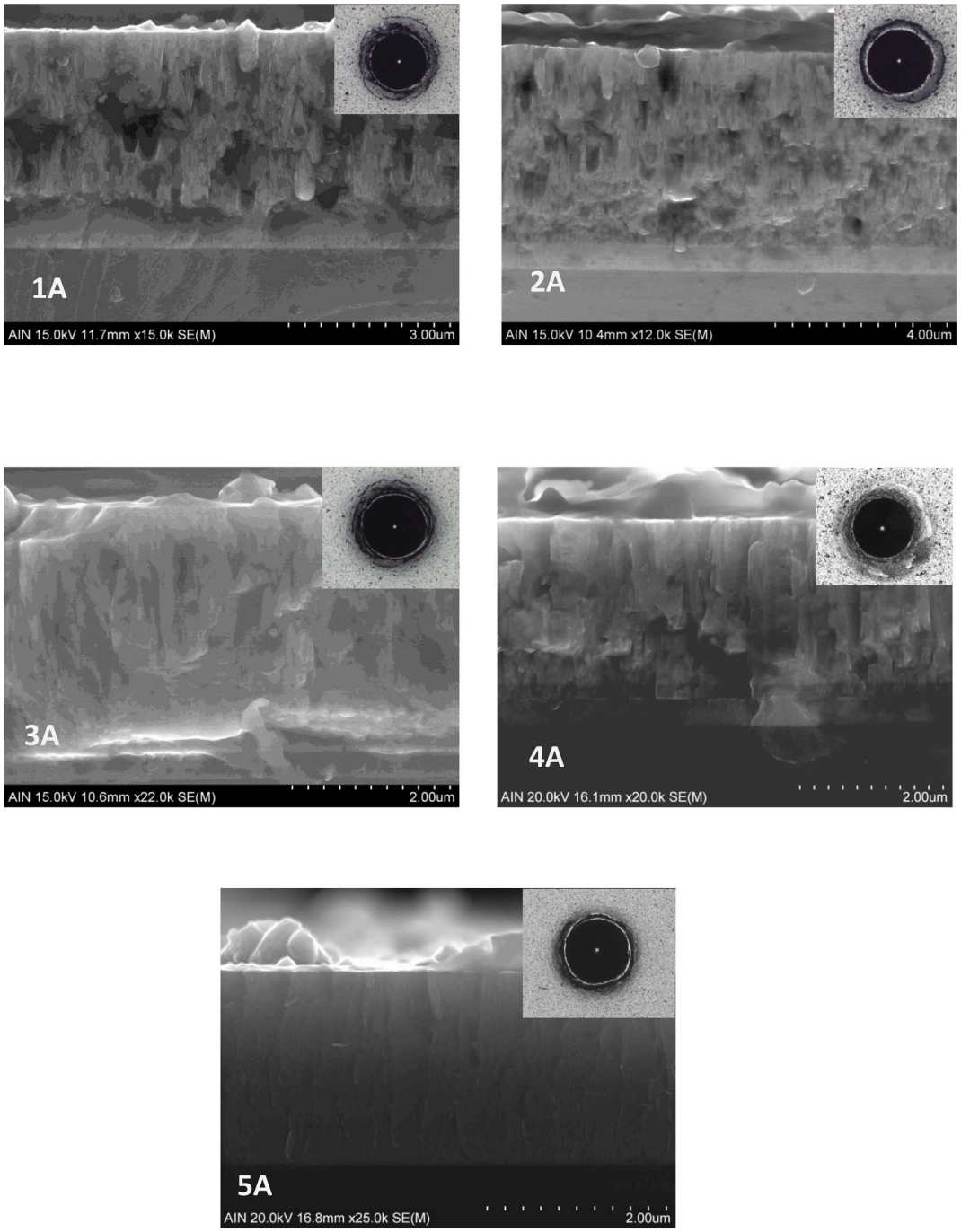

Fig. 1. SEM micrographs of the CrTiAlN films A-E in cross sectional view, as deposited on Si substrates. Top right insert represents the Rockwell C imprint on the coating substrate couple.

the 2θ regions 36–37°, 42–44° and 62–63° respectively. The specimens 4B, 4C and less clearly 5A reveal double peak structures. The low angle peaks of the doublets correspond to a lattice parameter of 0.424 nm, which can be attributed to unstrained TiN from the adhesion layer. The phases such as wurtzite-like AlN or other secondary phases (β-Cr_2N) were not identified. This all reveals that the coatings form well mixed solid solutions of fcc crystallographic structure. Fig. 3 shows the zoomed-in peak fit of the (002) diffraction peaks of the specimen **4D**, where the TiN and the solid solution features are identified. It can be also observed that the intensity of the peak features over background is smaller for the specimens with the largest Al content; i.e. specimens **4D** and **5A**.

Fig. 4 shows the corresponding fcc lattice parameters $\mathbf{a_0}$ as a function of the Aluminum atomic ratio, as measured over the peak position of the solid solution planes (002). The lattice parameters decrease as the Al at. % increases, which is in agreement with the fact that the incorporation of Al diminishes the average bond lengths of the cubic lattices, as reported in different studies, since the cubic Al—N bond length is the shortest among the other Me-N present (i.e. from 0.408 nm for c-AlN up to 0.414 nm for c-CrN and 0.424 nm for c-TiN). The same analyses were attempted as a function of the Cr at.%, Ti at.%, or even the Ti/Cr and Ti/Cr + Al [13], though no clear correlations could be observed for such large number of specimens. Even Fig. 4. exhibits some degree of dispersion due to the different concentrations of Ti and Cr in the coatings.

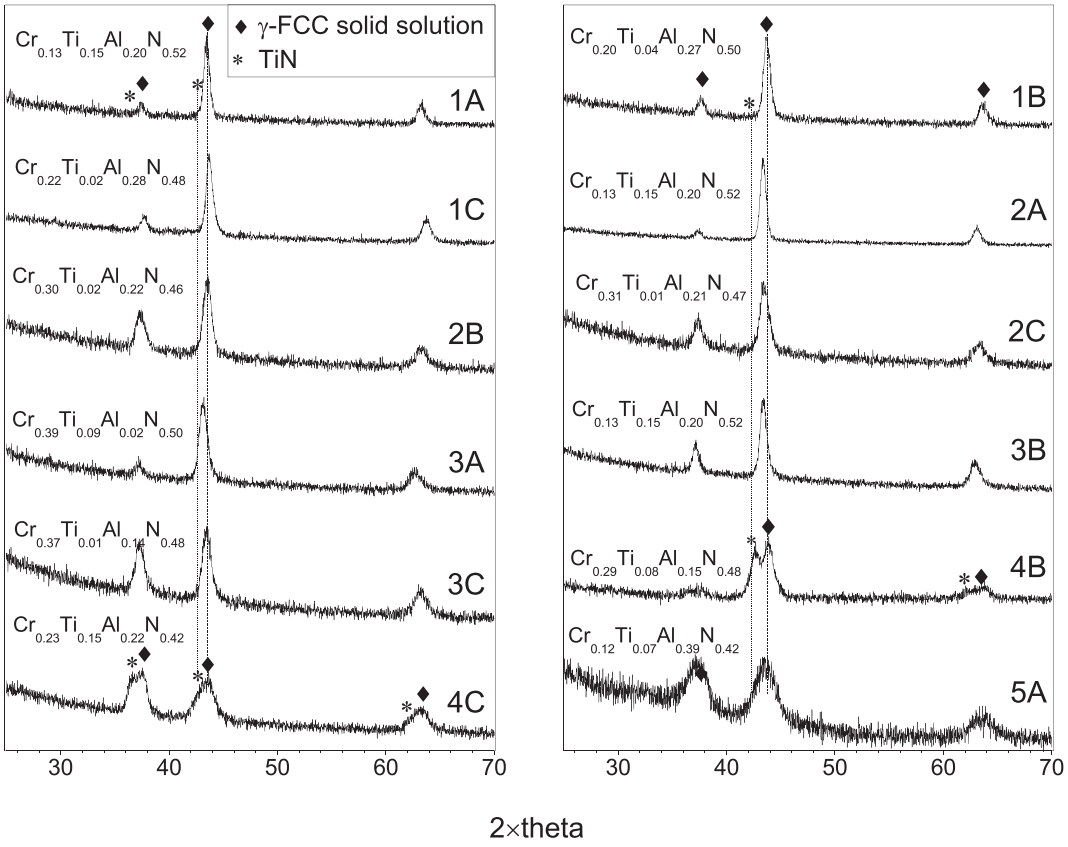

Fig. 2. X-ray diffraction patterns of the CrTiAlN specimens as labelled, measured at grazing angle.

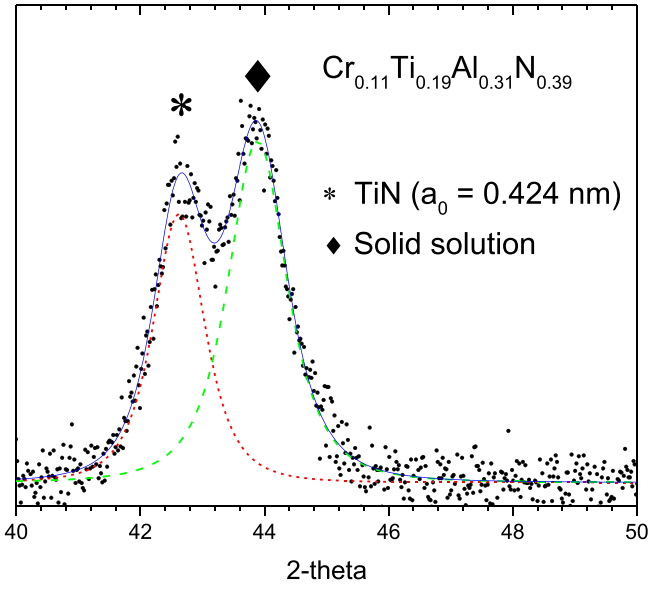

Fig. 3. Peak fit detail of the (002) XRD double reflection of the specimen 4D.

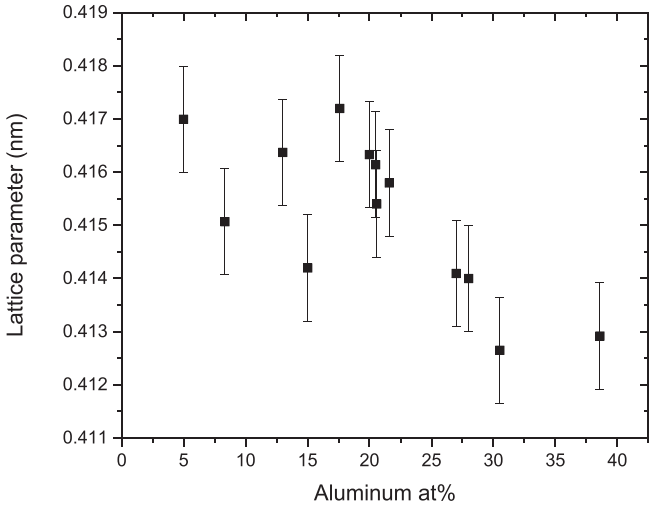

Fig. 4. Lattice parameter measured over the (002) diffractive plane for all specimens as a function of the Aluminum concentration.

3.2. *Indentation hardness and modulus: different dependencies*

In this section, the evolution of the indentation hardness and modulus of the coatings is analysed as a function of their compositions, in terms of different independent variables, (i) the Ti/Cr atom ratio, (ii) the total Al composition and (iii) the mix term of cation constituents. Fig. 5 shows the indentation hardness of the coatings as a function of the Ti/Cr cation ratio. The indentation hardness increases sharply as the Ti/Cr ratio increases from 0 up to 0.3. A dashed curve is added with the purpose to guide the eye. The observed trend might suggest that atomic fractions of Ti as small as 3–4 at.% in the current CrTiAlN coating structures are enough to raise the hardness to values in the range of AlTiN arc deposited coatings. Such evolution would agree with Xu et al. [9] who observed a sharp hardness increase of CAE deposited Al-Cr-N films as the Ti at.% raised to 10 and 18at%; specifically, from 27 GPa to 33 GPa, although with a modulus reduction. The increase of the indentation hardness as the Ti/Cr has also been found by other authors [7,10].

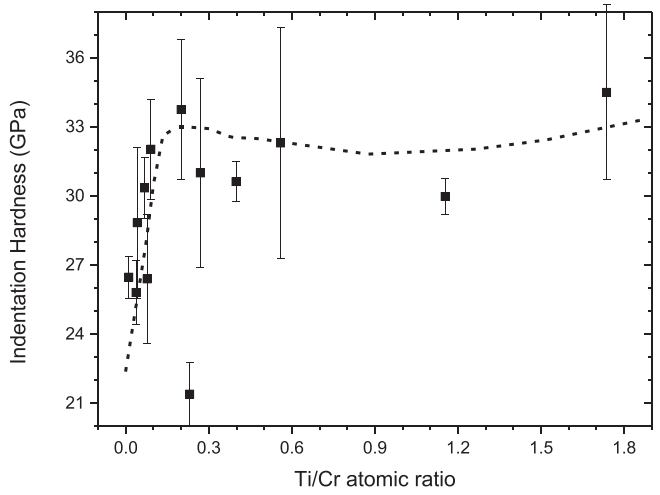

Fig. 5. Indentation hardness as a function of the Ti/Cr atom ratio.

The increasing hardness of the CrTiAlN coatings as the Ti/Cr ratio has been traditionally attributed to the fact that the extremes constituent of the quaternary system TiAlN or AlTiN are in general harder than these of the other extreme CrAlN or AlCrN [7,10]. On the other hand, other authors attributed the increase of the indentation hardness to solid solution strengthening as Ti is incorporated in the cation sites of the AlCrN solid solution [9]. However, a more detailed analysis of Fig. 5 reveals that the observed dependency of H on Ti/Cr is weak and not conclusive, in the context of the specimens used in this study. The main reason is that the increase of Titanium is normally concomitant to an increase of the Aluminum, due to the composition of the cathodes chosen.

In order to evaluate the influence of Aluminum on the indentation properties we have represented H as a function of the Al-at.%. This chose of the Al concentration as independent variable is justified first because Al has been found to be a strong driving factor of the lattice parameter (cf. Fig. 4); and on the other hand because it is well known the ability of Aluminum to increase the hardness of ternary TiAlN [31,32,33] and CrAlN [34,35] systems. Fig. 6 provides evidence of a strong effect of Al in the coating strengthening. It is observed how both modulus and hardness steadily and continuously (almost linearly) increase as Al-at.% increases. Again, the dispersion may arise to the fact that the coatings contain different amounts of Cr and Ti, and to the proper uncertainty of the measurements. It has to be pointed out that one of the coatings deviate strongly upon this behaviour, namely the specimen **5A**, which shows the largest Al content while its hardness reaches 27.8 GPa (cf. Table 3).

Whereas the effect of Al on the hardness of ternary compounds has been well reported [33–37], such dependency has not been found in the quaternaries CrTiAlN, to the best of our knowledge. This good correlation and the clear influence on the measured lattice parameters strongly suggest that the Al concentration may be tentatively ruling the mechanical properties of these quaternary coatings. This hardening effect is traditionally attributed in ternary coatings to solid solution strengthening. This is in fact a mechanism claimed classically to explain the hardening of multi component coatings [18,20,31,32] and of bulk materials [38]. On the other hand, and as well as in the case of the Ti/Cr factor, the increase of the Al, in most of the samples produced, also brings as side effect the increase of Ti. This fact, and the deviation observed for the specimen **5A** led us to explore another stoichiometric parameter which is able to verify the existence of solid solution strengthening beyond the mere 1-element increase (i.e. Aluminum or Ti).

Specifically, we have evaluated the hardness and modulus as a function of the 'mixing-up-ness' of the cation atoms Cr, Ti and Al. The rationale behind this approach is to explore whether the strengthening effect in a solid solution of *Z-type* atoms (Cr, Al, Ti and N in this specific case) is ruled by the number of equivalent permutes of the atoms all along the available lattice sites that give rise to the same macroscopic state. In a solid solution formation, the mixing of its elements yields a change of the configurational (molar) entropy of the system, with respect to the un-mixed state [19], which is equal to $-R\times\sum_i^N(\chi_i\times ln\chi_i)$, where χ_i represents the molar fraction of the *i*-th atom, and R is the universal gas constant. The mixing term maximizes when all their constituents are equimolar. Therefore, solid solution strengthening effects should manifest more remarkably as the mixing term maximizes.

Fig. 7 shows the indentation hardness of the CrTiAlN coating specimens represented as a function of the configuration term $-\sum_i^N\chi_i\times ln\chi_i$, (cf Table 3). Fig. 7 also shows the calculated residual in-plane film biaxial stresses as computed using the $\sin^2\psi$ method and the E' indentation values. We have plugged in the mixing formula only the metal cations concentrations as these conform the cation site scaffold of the cubic fcc solid solution. Either, adding N-atoms% in the mix term or normalizing the cation concentrations to the unity would only yield a re-scaling effect over the computed value of the mix term, with no

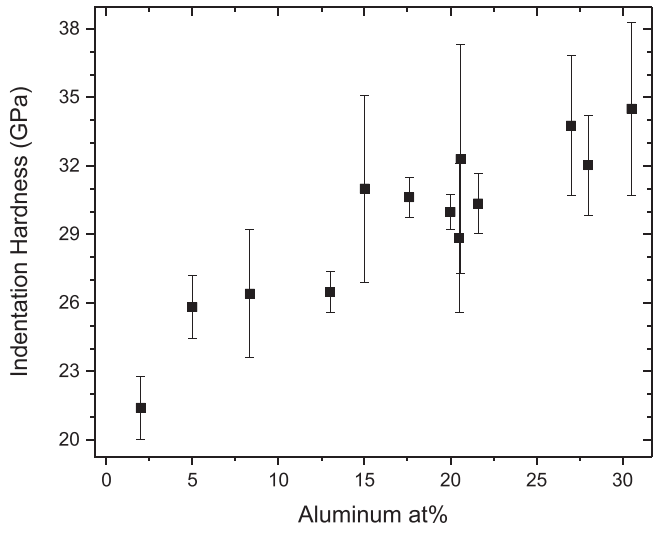

Fig. 6. Indentation hardness as a function of the Aluminum atomic/molar concentration.

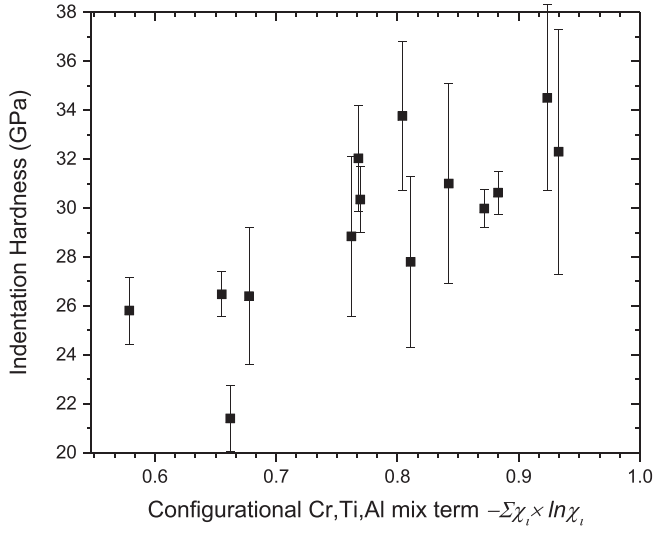

Fig. 7. Indentation hardness as a function of the solid solution mix term $-\sum_i^N\chi_i\times ln\chi_i$.

qualitative changes over the observed trends. It is evidenced in Fig. 7 how the indentation hardness of the quaternary CrTiAlN coatings also increase steadily as the mixing term increases. It can be also observed (not represented here) that the evolution of the indentation modulus also increases in a similar way (cf. Table 3), which is due to the internal stresses induced by the different lengths of the Me-N couples present (cubic Al—N, Cr—N and Ti—N). That causes the lattice structure to rigidize and to increase their elastic modulus. Indeed, a solid solution formed by various atomic species with different bond lengths lead to a distorted lattice structure. This lattice distortion causes local stress fields that jeopardize the displacement of the dislocations over their preferred slip crystal systems thus producing the macroscopic effect of strengthening [39].

The results shown here also agree with Xu et al. [9], although the small number of specimens did not allow an evaluation as this made in the present study. In addition, Zhou at al [7] also suggested the strengthening effect as underlaying the increase of hardness of CrTiAlN coatings as the Cr content increased. Even more, they observed a quasi-parabolic behaviour of the indentation hardness as a function of the Cr-target sputtering power, which they attributed as an increase of the softer CrN volume fraction in the coatings. Such behaviour is compatible with a direct dependency on the mix term as represented here, although according to their data, the maximal mix term does not coincide exactly with the maximal hardness [7], although the number of specimens studied was limited to 5.

The $\sin^2\psi$ evaluation of the films revealed compressive stress values ranging from −3 GPa down to −1 GPa, with no apparent correlation with the film thicknesses, thus suggesting that this parameter has not a determining role in the strengthening of the coatings. These values contrast with these of Chang et al. [40], who reported residual stresses of −7.5 GPa and − 7.9 GPa respectively for AlTiCrN/TiN and AlTiCrN/CrN coatings deposited by CAE. This difference could be explained in terms of the different deposition conditions. For example, the coatings of Ref [40] were deposited at lower temperatures (300 °C vs 450 °C), higher bias (−100 V vs −60 V) or the no Me-ion bombardment against the Ti^+ pre-bombardment (cf. phase 2 in the present study).

4. Conclusions

Quaternary CrTiAlN films were deposited by cathodic arc evaporation using a combinatorial approach of cathode compositions. All the coatings exhibited solid solution lattice structures regardless of their composition. The microscopical and adhesion tests revealed dense columnar microstructures with a good bonding to the H13 steel substrates respectively. The lattice parameter of the coating solid solutions reveals a clear downwards dependency as the absolute Aluminum concentrations increase.

The dependencies of the indentation hardness and modulus have been unveiled in terms of the stoichiometries and crystalline structures of the films. The Ti/Cr and the total Al% exhibit a notable influence over the hardnesses and moduli of the coatings, which has been traditionally attributed to a solid solution strengthening effect, both in ternary and quaternary systems. However, neither the Ti/Cr nor the Aluminum content alone provide full evidence of this hardening mechanism since 1-element variation does not allow a broad view over the hardness dependencies as a function of a comprehensive multielement compositional map.

In order to confirm that the underlaying mechanical response of the coatings is solid solution strengthening, the indentation hardness has been evaluated as a function of the multielement mixing term $-\sum_i^N(\chi_i \times ln\chi_i)$. From the observed increase of the hardness and modulus as the mixing term increases and taking into account that (1) all films crystalline structures are compatible with solid solutions, i.e. no other phases were observed and (2) the film residual stress seemed not to show any clear trend upon the stoichiometries; it can be confirmed that the solid solution strengthening mechanisms fully determines the mechanical response of this quaternary system.

CRediT authorship contribution statement

Gonzalo G. Fuentes: Project conceptualization, design of experiments, writing, editing and submission. **Lucía Pérez.:** PVD sample preparation, GDOES and indentation hardness measurements. **José Fernández Palacio**: XRD measurements. **Angel Medrano**: PVD set up, process parameterization. Eduardo Arias: XRD analyses, stress measurements, and final editing. **Rebeca Bueno:** SEM and rockwell C tests. **Jonathan Fernández**: Scientific discussion, final editing and revision.

Declaration of competing interest

The authors declare that they have no known competing financial interests or personal relationships that could have appeared to influence the work reported in this paper.

Acknowledgements

This work has been funded by the Spanish Ministry of Science and Innovation of Spain through the project PGC2018-096855-A-C44. The authors also acknowledge the *Centro para el Desarrollo Tecnológico e Industrial* (CDTI) for the support of the excellence program CERVERA through the project CER2019-1003.

References

[1] G.S. Fox-Rabinovich, A.I. Kovalev, M.H. Aguirre, B.D. Beake, K. Yamamoto, S. C. Veldhuis, J.L. Endrino, D.L. Wainstein, A.Y. Rashkovskiy, Surface & Coatings Technology 204 (2009) 489–496.
[2] Lijing Bai, Xiaodong Zhu, Jiming Xiao, Jiawen He, Surface & Coatings Technology 201 (2007) 5257–5260.
[3] K. Yamamoto, T. Sato, K. Takahara, K. Hanaguri, Surf. Coat. Technol. 174–175 (2003) 620–626.
[4] K.E. Cooke, S. Yang, C. Selcuk, A. Kennedy, D.G. Teer, D. Beale, Development of duplex nitrided and closed field unbalanced magnetron sputter ion plated CrTiAlN-based coatings for H13 aluminium extrusion dies, Surf. Coat. Technol. 188–189 (2004) 697–702.
[5] G.S. Fox-Rabinovich, K. Yamomoto, S.C. Veldhuis, A.I. Kovalev, G.K. Dosbaeva, Tribological adaptability of TiAlCrN PVD coatings under high performance dry machining conditions, Surf. Coat. Technol. 200 (2005) 1804–1813.
[6] Jianliang Lin, Xuhai Zhang, Yixiang Ou, Ronghua Wei. Surface & Coatings Technology 277 (2015) 58–66.
[7] Z.F. Zhou, P.L. Tam, P.W. Shum, K.Y. Li, Thin solid films 517 (2009) 5243–5247.
[8] T. Yamamoto, H. Hasegawa, T. Suzuki, T.K. Yamamoto, Surface & Coatings Technology 200 (2005) 321–325.
[9] Yuxiang Xu, Li Chen, Fei Pei, Yong Du, Influence of Ti on the mechanical properties, thermal stability and oxidation resistance of Al–Cr–N coatings vacuum 120 (2015) 127–131.
[10] M. Danek, F. Fernandes, A. Cavaleiro, T. Polcar, Influence of Cr additions on the structure and oxidation resistance of multilayered TiAlCrN films, Surf. Coat. Technol. 313 (2017) 158–167.
[11] H. Hasegawa, T. Yamamoto, T. Suzuki, K. Yamamoto, The effects of deposition temperature and post-annealing on the crystal structure and mechanical property of TiCrAlN films with high Al contents, Surf. Coat. Technol. 200 (2006) 2864–2869.
[12] Y.H. Chen, L. Rogström, D. Ostach, N. Ghafoor, M.P. Johansson-Jõesaar, N. Schell, J. Birch, M. Odén, Effects of decomposition route and microstructure on h-AlN formation rate in TiCrAlN alloys, J. Alloys Compd. 691 (2017) 1024–1032.
[13] Argyrios Georgiadis, Gonzalo G. Fuentes, Eluxka Almandoz, Angel Medrano, José F. Palacio, Adrián Miguel, Characterisation of cathodic arc evaporated CrTiAlN coatings tribological response at room temperature and at 400°C, Mater. Chem. Phys. 190 (2017) 194e201.
[14] Qianzhi Wang, Fei Zhou, Jiwang Yan. Surface & Coatings Technology 285 (2016) 203–213.

[15] Cheng-Hsun Hsu, Kai-Lin Chen, Chun-Ying Lee, Kuan-Chain Lu, Thin Solid Films 518 (2010) 3825–3829.
[16] A. Alberdi, M. Marín, B. Díaz, O. Sánchez, R. Escobar Galindo, Vacuum 81 (2007) 1453–1456.
[17] F. Fernandes, M. Danek, T. Polcar, A. Cavaleiro, Tribological and cutting performance of TiAlCrN films with different Cr contents deposited with multilayered structure, Tribol. Int. 119 (2018) 345–353.
[18] D. Diechle, M. Stueber, H. Leiste, S. Ulrich, V. Schier, Combinatorial approach to the growth of α-(Al_{1-x},Cr_x)2O3 solid solution strengthened thin films by reactive r.f. magnetron sputtering, Surface & Coatings Technology 204 (2010) 3258–3264.
[19] Metallurgical thermodynamics. D.R. Gaskell in Physical Metallurgy Part 1. Edited by R.W. Cahn and P. Haasen. North-Holland Physics Puplishing (1983).
[20] Wei Li, Ping Liu, Peter K. Liaw, Microstructures and properties of high-entropy alloy films and coatings: a review, Math. Res. Lett. 6 (4) (2018) 199–229.
[21] W. Chen, An Yan, Xianna Meng, Dongquing Wu, Dencan Yao, Daoda Zhang, Microstructural change and phase transformation in each individual layer of a nano-multilayered AlCrTiSiN high-entropy alloy nitride coating upon annealing, Appl. Surf. Sci. 462 (2018) 1017–1028.
[22] Jörg Vetter, Wolfgang Burgmer, J. Anthony, Arc-enhanced glow discharge in vacuum arc machines, Perry. Surface and Coatings Technology 59 (1993) 152–155.
[23] J. Fernández de Ara, E. Almandoz, J.F. Palacio, G.G. Fuentes, R.J. Rodríguez, J. A. García, Surface & Coatings Technology 258 (2014) 754–762.
[24] W. Oliver, G. Pharr, J. Mater. Res. 19 (1) (2004) 3–20.
[25] Gonzalo G. Fuentes, Eluxka Almandoz, Rafael J. Rodríguez, Hanshan Dong, Yi Qin, Sonia Mato, Francisco Javier Pérez-Trujillo, Manufacturing Rev. 1 (2014) 20.
[26] G.G. Fuentes, R. Rodriguez, J.C. Avelar-Batista, J. Housden, F. Montalá, L. J. Carreras, A.B. Cristobal D, J.J. Damborenea, T.J. Tate, J. Materials Processing Technology 167 (2005) 415–421.
[27] L. Hultman, Thermal stability of nitride thin films, Vacuum 57 (2000) 1–30.
[28] M. Jílek, M. Jílek, F. Mendez Martin, P.H. Mayrhofer, S. Veprek, High-rate deposition of AlTiN and related coatings with dense morphology by central cylindrical direct current magnetron sputtering, Thin Solid Films 556 (2014) 361–368.
[29] C. Sabitzer, J. Paulitsch, S. Kolozsvári, R. Rachbauer, P.H. Mayrhofer, Influence of bias potential and layer arrangement on structure and mechanical properties of arc evaporated Al–Cr–N coatings, Vacuum 106 (2014) 49–52.
[30] A.E. Reiter, V.H. Derflinger, B. Hanselmann, T. Bachmann, B. Sartory, Investigation of the properties of $Al_{1-x}Cr_xN$ coatings prepared by cathodic arc evaporation, Surf. Coat. Technol. 200 (2005) 2114–2122.
[31] S. PalDey, S.C. Deevi, Single layer and multilayer wear resistant coatings on (Ti,Al) N: a review, Mater. Sci. Eng. A 342 (2003), 58e79.
[32] D. Rafaja, V.Klemm M.Šíma, G. Schreiber, D. Heger, L. Havela, R. Kužel, X-ray diffraction on nanocrystalline Ti1−xAlxN thin films, J. Alloys Compd. 378 (2004) 107–111.
[33] Zongjian Liu, P.W. Shum, Yongfeng Shen. Hardening mechanisms of nanocrystalline Ti–Al–N solid solution films. Thin Solid Films 468(1):161–166.
[34] D. Diechle, M. Stueber, H. Leiste, S. Ulrich, Combinatorial approach to the growth of α-$(Al_{1-x},Cr_x)_{2+\delta}(O_{1-y},N_y)_3$ solid solution strengthened thin films by reactive r.f. magnetron sputtering, Surf. Coat. Technol. 206 (2011) 1545–1551.
[35] Z.B. Qia, Z.T. Wu, Z.C. Wang, Improved hardness and oxidation resistance for CrAlN hard coatings with Y addition by magnetron co-sputtering, Surf. Coat. Technol. 259 (2014) 146–151.
[36] P.L. Tam, Z.F. Zhou, P.W. Shum, K.Y. Li, Structural, mechanical, and tribological studies of Cr–Ti–Al–N coating with different chemical compositions, Thin Solid Films 516 (2008) 5725–5731.
[37] A.E. Reiter, V.H. Derflinger, B. Hanselmann, T. Bachmann, B. Sartory, Investigation of the properties of $Al_{1-x}Cr_xN$ coatings prepared by cathodic arc evaporation, Surf. Coat. Technol. 200 (2005) 2114–2212.
[38] Pengfei Ma, Shibo Li, Jie Hu, Xiaogang Lu, Wenbo Yu, Yang Zhou, Processing and characterization of $MoAl_{1-x}Si_xB$ solid solutions, J. Alloys Compd. 814 (2020), 152290.
[39] Indranil Basu, Jeff T.H.M. De Hosson, Strengthening mechanisms in high entropy alloys: fundamental issues, Scr. Mater. 187 (2020) 148–156.
[40] Yin-Yu Chang, Yu-Ju Yanga, Shi-Yao Weng. Surface & Coatings Technology 389 (2020) 125637.